DOI: 10.1002/anie.201006639

Catalyst–Support Interactions

Dissolved Carbon Controls the Initial Stages of Nanocarbon Growth**

Ali Rinaldi, Jean-Philippe Tessonnier, Manfred E. Schuster, Raoul Blume, Frank Girgsdies, Qiang Zhang, Timo Jacob, Sharifah Bee Abd Hamid, Dang Sheng Su,* and Robert Schlögl*

Carbon is a versatile material that, depending on its hybridization and assembly in one-, two-, or three-dimensional networks, exhibits important electronic and chemical properties with countless practical applications. For example, it is found in printer inks, pencils, water purification systems, thermal isolation, and antistatic materials.[1–3] More elaborate carbon materials, such as carbon nanotubes, are also employed in nanotechnology, with applications in sensing or field emission.[4] Carbon black is cheap, easy to synthesize, and easy to modify.[4] Thus, it is also particularly suited as a support for heterogeneous catalysis as both the structure (macroscopic shape, porosity) and the surface chemistry can be tailored depending on the target application.[4]

In catalysis, the support is known to act on heat and mass transfer, but also on the active phase through strong metal–support interactions (the SMSI effect).[5] In the case of black carbon, the structural order (graphitic character) adds one level of complexity but also one degree of freedom for logical catalyst design. It is of crucial importance to study how the graphitic character influences the anchoring of the nanoparticles and eventually modifies the catalytic activity of the metal. Varying the graphitic order might offer new and fascinating possibilities for catalyst design.

Herein we probe the metal–carbon support interaction by growing carbon nanotubes. Their observation by high-resolution transmission electron microscopy (HRTEM) yields direct information on the state of the active phase and in particular on a possible support effect. We anticipate that these results can also be extended to the growth of graphene. The nanotubes were grown by catalytic chemical vapor deposition (CCVD) of ethylene on nickel catalysts supported on two vapor-grown carbon fibers (VGCFs). VGCFs have a layer of disordered pyrolitic carbon on their surface, which can be graphitized by annealing at high temperature. Thus, supports with identical morphologies but different graphitic character can be easily synthesized. Herein, we used supports annealed at 1073 K (defective carbon) and at 3000 K (graphitic carbon). The pristine supports were not chemically modified to prevent any influence from surface chemistry on the catalytic activity of the Ni particles.

After reduction, the Ni/defective carbon (Ni/dC) and Ni/graphitic carbon (Ni/gC) samples were both exposed to ethylene and hydrogen at 973 K to grow carbon nanotubes. HRTEM images (Figure 1, Supporting Information, S3) show that strongly disordered carbon nanofibers (CNFs) grew on the Ni/dC sample, whereas Ni/gC led to quasi-perfect multiwall carbon nanotubes (MWCNTs). It should be noted that the carbon nanofilaments (CNFs and MWCNTs) always grew in accordance with the tip-growth mechanism.

The Ni nanoparticles, which catalyze the growth of the nanofilaments, detach from the support in the early stages of the reaction. Therefore, the observed phenomenon cannot be simply explained by the differences in metal–support interaction (the SMSI effect), or at least not as it is traditionally defined. The interaction of the nickel particles with the carbon supports modified the nickel either before exposure to ethylene or in the early stages of the catalytic reaction, thus determining whether CNFs or MWCNTs are grown.

By combining several in situ characterization techniques with HRTEM and theoretical calculations, we aimed to identify the origins of the observed structural differences in the nanofilament product. Obvious parameters, such as nickel particle size and shape, could be ruled out by HRTEM (Supporting Information, S4). Microstructural and crystallographic investigations involving HRTEM and in situ X-ray diffraction (XRD) techniques were carried out on the two supported catalysts after reduction at 573 K in hydrogen and further heating to 973 K in an inert gas (Figure 1).

Before growth, both techniques agreed on the presence of face-centered-cubic nickel for the two supported catalysts. However, in the case of the Ni/dC sample, broad and asymmetric nickel diffraction peaks were observed after reduction. The Ni(111) and (200) peaks at 44.5° and 52°, respectively (the latter is not shown), both exhibited a shoulder at higher d values (Figure 1g). These shoulders shifted to 43.7° and 50.7° and were better resolved after the catalyst was exposed to ethylene. There is no known phase found to match these additional peaks. We therefore suggest that the splitting of the Ni(111) and Ni(200) peaks is most

[*] A. Rinaldi, Dr. J.-P. Tessonnier, Dr. M. E. Schuster, Dr. R. Blume, Dr. F. Girgsdies, Dr. Q. Zhang, Prof. Dr. D. S. Su, Prof. Dr. R. Schlögl
Fritz-Haber-Institut der Max-Planck-Gesellschaft
Faradayweg 4–6, 14195 Berlin (Germany)
Fax: (+49) 30-8413-4401
E-mail: dangsheng@fhi-berlin.mpg.de
Dr. T. Jacob
Universität Ulm
Albert-Einstein-Allee 47, 89081 Ulm (Germany)
E-mail: timo.jacob@uni-ulm.de
Prof. Dr. D. S. Su
Shenyang National Laboratory for Materials Science
Institute of Metal Research, Chinese Academy of Science
72 Wenhua Road, Shenyang 110016 (China)
Prof. S. B. Abd Hamid
Combicat, University of Malaya
Kuala Lumpur 50603 (Malaysia)

[**] T.J. gratefully acknowledges support by the Deutsche Forschungsgemeinschaft (DFG) within the Emmy-Noether-Program.

Supporting information for this article is available on the WWW under http://dx.doi.org/10.1002/anie.201006639.

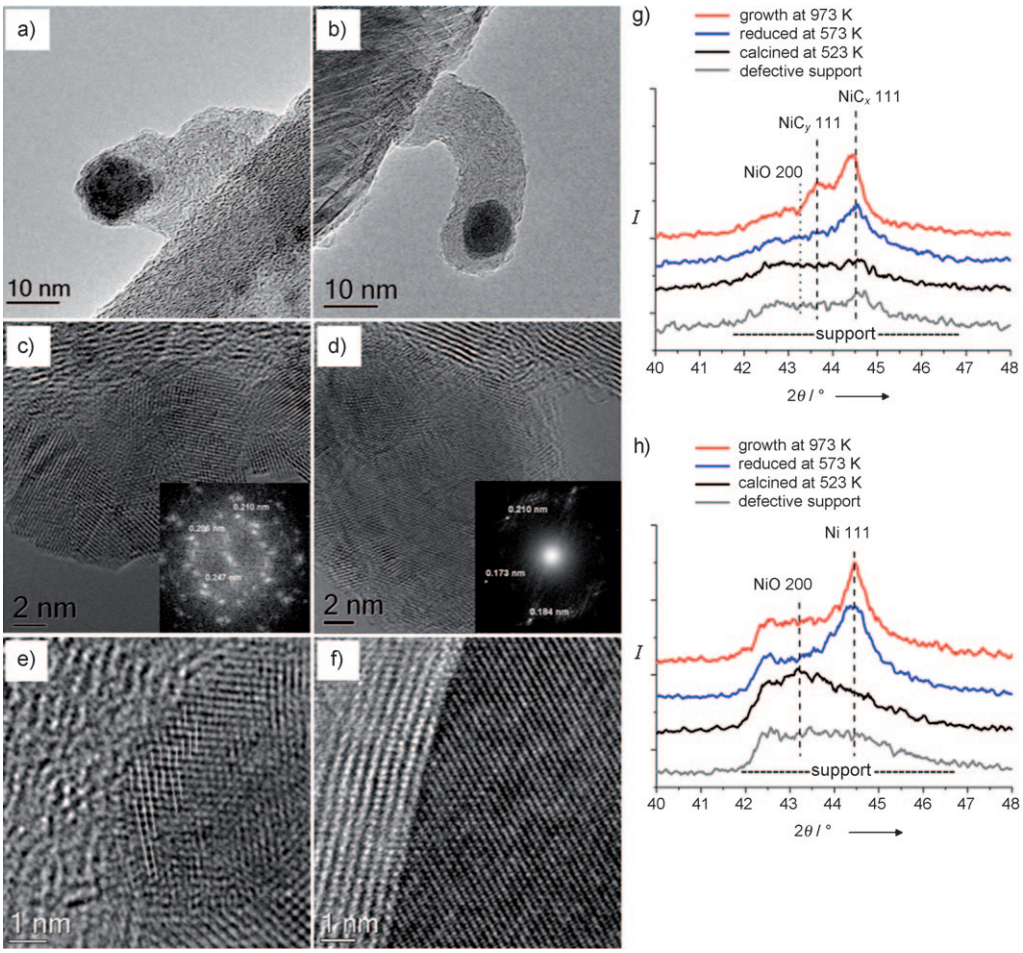

Figure 1. TEM images of a CNF and CNT grown from a) Ni/defective carbon (Ni/dC) and from b) Ni/graphitic carbon (Ni/gC). Aberration-corrected HRTEM images of the two catalysts after reduction at 573 K and ramping in inert gas to 973 K reveal that nickel nanoparticles supported on defective carbon are polycrystalline (c) with many regions with strain and dislocations (e). In contrast, the nickel lattice in graphitic carbon supported particles is well-ordered (d,f). In situ XRD experiments show that the polycrystallinity is a result of atomic carbon incorporation from the defective support (g). In the case of Ni/gC, the nanoparticles remain in the metallic state (h). (Diffractograms in (g) and (h) are vertically shifted.)

likely caused by carbon from the defective support dissolving in the nickel lattice, resulting in its expansion, as already observed for carbon dissolution in bulk nickel.[6,7] The result is a carbidic nickel, referred to below as NiC$_x$.[8,9] HRTEM further supports this interpretation, as a bimodal distribution of d spacings is observed for this sample (Figure 1e and Supporting Information, S5). For comparison, in situ XRD and HRTEM investigations show that nickel on graphitic carbon remains in its metallic state throughout the experiment. The particles exhibit well-stacked rows of nickel atoms, thus forming large quasi defect-free domains (Figure 1d and f). Furthermore, experimental d values from HRTEM images are in good agreement with those provided from crystallographic databases for metallic nickel ($d_{[111]} = 0.2034$ nm).

To better understand the incorporation of carbon atoms into nickel, which can also be viewed as the initial stages of NiC$_x$ formation, we performed DFT calculations on the adsorption of carbon atoms on Ni(111) and Ni(100), followed by subsequent studies on the diffusion into the surface. Ni(111) represents the close-packed surface orientation, which can be expected to dominate nanoparticle surfaces, whereas Ni(100) represents a more open surface. For all studies, a coverage of 0.25 ML has been assumed, which gave the surface atoms enough freedom to rearrange during sub-surface diffusion. Carbon penetrates into the Ni(111) surface (see Figure 2a and Supporting Information, S6 for details) and migrates to octahedral subsurface sites, with an effective energy barrier of 1.92 eV, which is comparable to an experimental value of (1.9 ± 0.1) eV.[8]

Interestingly, by carbon diffusing into the surface, the system gains 0.29 eV per carbon atom, showing that even the surface carbide formation is a thermodynamically favorable process. In addition to Ni(111) planes, nanoparticles also offer a variety of low-coordinate sites for carbon adsorption or absorption. We therefore investigated carbon diffusion into the Ni(100) plane (Figure 2a). The energetic barrier is calculated to be 1.45 eV, which agrees with the measured value of (1.4 ± 0.1) eV.[8] Near lower-coordinate nickel surface sites or defects, which are expected to be of particular relevance for nanoparticles, we would even expect much lower energy barriers, an effect that has been confirmed recently.[10] Figure 2b shows the localized density of states for nickel atoms of the first and second surface layers and also for carbon.

Comparing the systems of adsorbed and absorbed carbon shows that on both Ni(100) and Ni(111) surfaces the carbon p states are stabilized when diffusing into the surfaces. This behavior is accompanied by a slight upward shift of the d states of surface nickel atoms, whereas nickel atoms of the second surface layer are almost unaffected. Therefore, carbon diffusion into the surface leads to pronounced changes of the localized density of states. These changes mainly modify the electronic structure of the surface, and thus the catalytic activity of the Ni/NiC$_x$ particles.

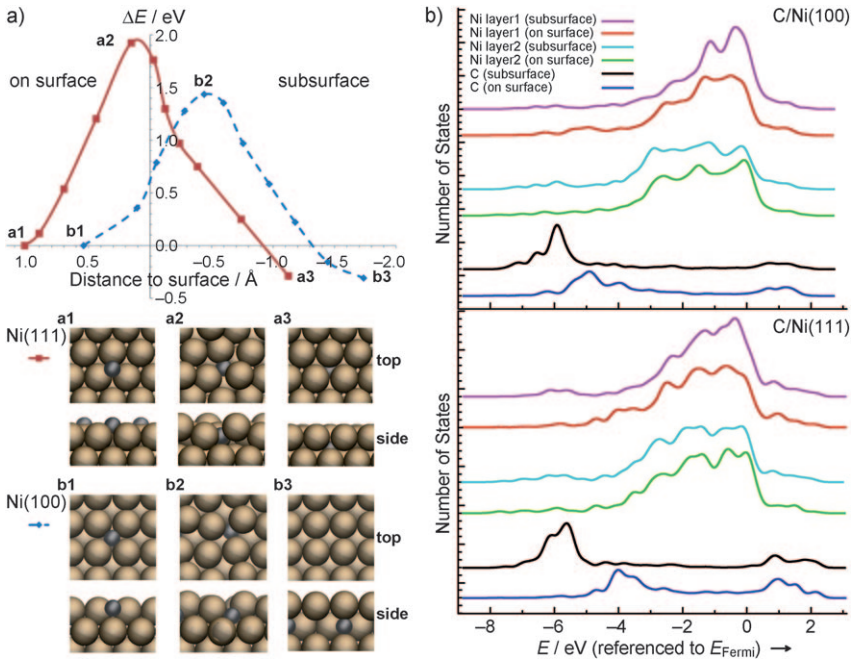

Figure 2. a) Top: Energy as a function of the distance of carbon to the Ni(100) and Ni(111) surfaces (in each case referenced to the adsorbed system). Bottom: Plan and side views of the Ni(100) and Ni(111) surfaces during the diffusion process. **a1** and **b1** show the adsorbed systems, **a2** and **b2** the transition states, and **a3** and **b3** the systems with subsurface carbon. b) Density of states for carbon adsorbed (on surface) and absorbed (subsurface) on/into Ni(100) and Ni(111). For each system, Ni atoms of the first two surface layers and the carbon atoms were analyzed. Whereas the nickel states have mostly d character, the carbon states have p character. (Spectra in (b) are vertically shifted.)

The defective support exhibits a large amount of non-aromatic carbon on the surface, which could easily diffuse into the supported nickel particles because of the high difference in chemical potential between both. However, in the case of the graphitic support, carbon atoms have to be first extracted from perfect graphene sheets, which is only possible by overcoming a high energy barrier (calculated to be above 3 eV). This barrier is high enough to prevent carbon extraction from graphene sheets, which explains why only very little NiC_x is observed for Ni/gC.

To gain insight into the possible carbon incorporation, the nickel-based catalysts were investigated by means of in situ X-ray photoelectron spectroscopy (XPS) to observe the evolution of the active phase during reduction and consecutive nanofilament growth (Figure 3). The Ni 2p peak can be fitted with two contributions, corresponding to metallic nickel (852.6 eV) and NiC_x (853.5 eV). The NiC_x to metallic nickel ratio differed for both samples after reduction at 573 K and ramping in inert atmosphere to 973 K.

While metallic nickel was the dominant phase for Ni/gC, Ni/dC exhibits a significantly higher NiC_x contribution prior to the exposure to ethylene (Figure 3c). As the only available carbon source was the catalyst support itself, these experiments further confirmed the role played by the support in the NiC_x formation. Both in situ XRD and XPS showed that carbon incorporation already started during reduction (Figure 1g, 3a and c) and continued while ramping to 973 K in an inert atmosphere (Figure 3a and c).

The carbon diffusion is more likely to start at the metal–carbon support interface. Indeed, strains and dislocations in the nickel fcc structure were present in this interfacial region (Figure 1e). Furthermore, previous investigations report the occurrence of dislocations and strain upon carbon incorporation in nickel.[7,11,12] Surprisingly, we did not observe any encapsulation of the nickel nanoparticles with carbon after cooling to room temperature. This result suggests that the nickel–carbon compound is relatively stable and that carbon is not ejected from the particle, which is in agreement with our calculations.

It is also noteworthy that the amount of dissolved carbon measured by XRD and XPS after growth was significantly different for both samples (Figure 1 and Figure 3). While carbon further dissolves in Ni/dC under the reaction conditions, Ni/gC remains in its metallic state. For the latter, the NiC_x contribution in the XP spectrum is expected to mainly come from the interface between the nickel particle and the grown MWCNT, which raises questions about the role of dissolved carbon on the CNT growth mechanism. The majority of our results agree with the works of Helveg et al.[13] and of Hofmann et al.,[14] showing that ethylene is first dissociated on the metallic nickel surface, followed by the surface diffusion of carbon atoms and finally assembling to grow a CNT. However, the surface sensitivity of the techniques we employed showed that the CNTs actually grew from a surface carbide (carbide layer on top of a bulk metallic nickel particle) instead of from purely metallic nickel. Nevertheless, bulk carbidic nickel, as in the case of the nickel/defective carbon, does not form. Therefore, we conclude that the growth of either CNFs or CNTs can be directly linked with carbon incorporation (sub-surface) in the nickel particles during the activation of the catalyst (Figure 4).

We have conducted dosing experiments with ethylene at a low temperature on Ni/gC to test this hypothesis. At a low temperature part of the pulsed ethylene dissociates on the surface of the nickel particles to form carbon deposits, which should simulate the defective carbon support. In situ XP spectra showed that carbon was not incorporated in nickel instantly after pulsing ethylene at 673 K but actually diffused into the sub-surface during further heating to 973 K in an inert gas (Figure 5b and 3c). Nanofilaments grown at 973 K exhibit a disordered structure, similar to filaments grown on Ni/dC (Figure 5a).

Our work highlights the ways carbon supports influence the catalytic activity of transition-metal particles located on their surface. So far, the role of oxygen-containing surface functional groups was expected to explain observed differences in catalytic activity. From our work, we demonstrate

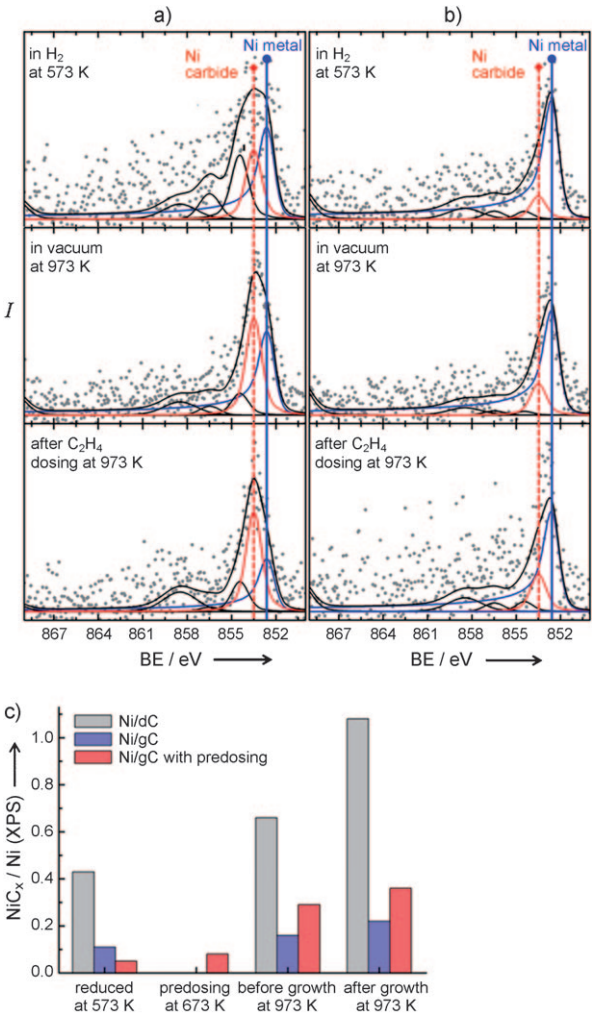

Figure 3. Evolution of the Ni2p XP spectra for Ni/dC (a) and Ni/gC (b) after reduction, heating to growth temperature in inert gas, and exposure to the reaction feed. The NiC_x/Ni ratio increase significantly when nickel is supported on defective carbon or when nickel is exposed to ethylene pre-dosing at low temperatures (c).

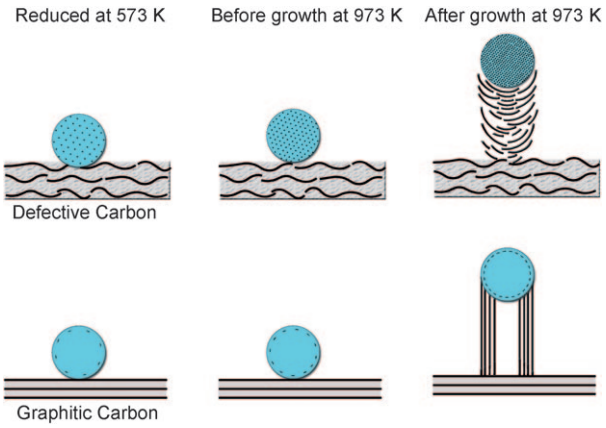

Figure 4. The growth of nanocarbon from carbon-supported nickel catalyst. C light blue, C black/gray.

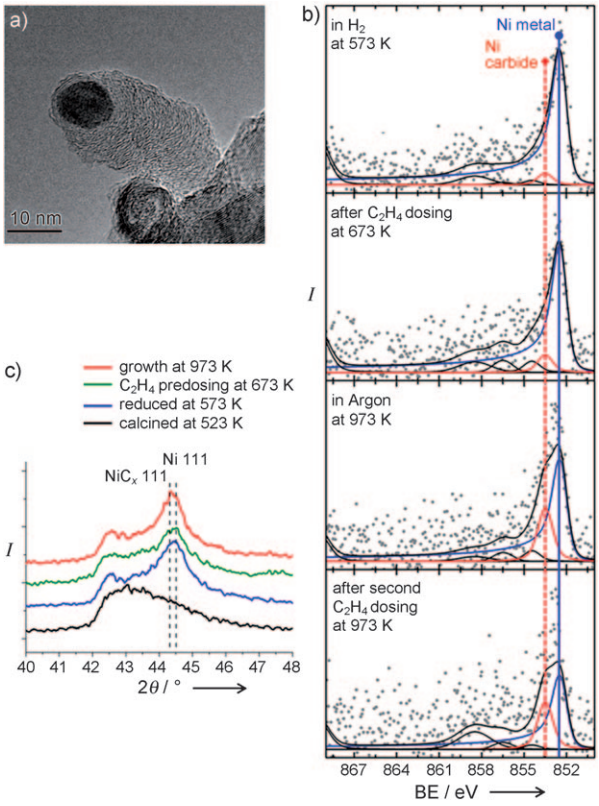

Figure 5. TEM image of a CNF grown on nickel supported on graphitic carbon with ethylene predosing at 673 K prior to growth at 973 K (a). Evolution of the Ni2p spectra for Ni/gC after reduction, after ethylene dosing at 673 K and after heating to 973 K and after growth (b). In situ XRD pattern of Ni/gC after reduction, predosing, and growth (c). (Spectra in (c) are vertically shifted.)

that defective carbon also plays a dramatic role. In the present case, it was possible to grow either CNFs or MWCNTs by simply introducing carbon atoms into the nickel particles prior to growth. Carbon atoms can either be provided by the support or by exposing the catalyst to hydrocarbons at a relatively low temperature (Figure 3). Furthermore, the subsurface carbon species formed after pre-dosing with ethylene were stable under reaction conditions. The growth of CNFs instead of MWCNTs on nickel particles, in which carbon has been incorporated at low temperature, can be explained by both electronic and structural effects. As shown in Figure 2b, carbon incorporation leads to a shift in the density of states which obviously modifies the catalytic activity of the nickel atoms. Furthermore, the diffusion of carbon in the nickel particles induced their reconstruction (Figure 1c). The particles became polycrystalline, with faces oriented in various directions. During growth, small graphene sheets most likely formed on each of the faces and interconnected in a random way, thus leading to a soot-like structure.

These experiments lead to three major conclusions. First, it is now clear that differences in catalytic activity observed for the past 50 years for metals supported on various carbons can be partially explained by carbon incorporation from the support. The amount of introduced carbon remains relatively low and might only be observed with highly sensitive in situ

techniques, which explains why such an effect has not been demonstrated before. We expect that carbon incorporation might explain differences observed, for example for ammonia decomposition on Ru/C or hydrogenation reactions with Pd/C. For the latter, Teschner et al. observed a PdC_x signal by in situ XPS on a freshly prepared Pd/CNT catalyst that gave a higher selectivity in the pentyne hydrogenation reaction than Pd/Al_2O_3.[15] Second, we observed carbon incorporation already during reduction at 573 K, which is an activation condition typical for catalysts. Therefore, carbon incorporation may also play a role for reactions occurring at low temperatures. Finally, we saw that it is possible to also introduce sub-surface carbon by exposing the active metal to hydrocarbons at low temperature. This offers new possibilities to control the catalytic activity of metal particles and might open new routes for the rational design of heterogeneous catalysts.

Received: October 22, 2010
Published online: February 24, 2011

Keywords: carbon nanotubes · dissolved carbon · nanoparticle catalysts · nickel · supported catalysts

[1] O. Vohler, F. von Sturm, E. Wege, H. von Kienle, M. Voll, P. Kleinschmitt in *Ullmann's Encyclopedia of Industrial Chemistry*, VCH, Weinheim, **1986**.
[2] J. Donnet, R. C. Bansal, M. Wang, *Carbon Black*, CRC, Boca Raton, **1993**.
[3] H. Marsh, F. Rodríguez-Reinoso, *Activated Carbon*, Elsevier, Dordrecht, **2006**.
[4] P. Serp, J. L. Figueiredo, *Carbon Materials for Catalysis*, Wiley, Hoboken, **2008**.
[5] S. J. Tauster, S. C. Fung, R. T. K. Baker, J. A. Horsley, *Science* **1981**, *211*, 1121 – 1125.
[6] L. Zwell, E. Fasiska, Y. Nakada, A. Keh, *Trans. Metall. Soc. AIME* **1968**, *242*, 765 – 766.
[7] V. K. Portnoi, *Phys. Met. Metallogr.* **2010**, *109*, 153 – 161.
[8] A. Wiltner, C. Linsmeier, T. Jacob, *J. Chem. Phys.* **2008**, *129*, 084704.
[9] Y. Zhao, C. Bowers, I. Spain, *Carbon* **1988**, *26*, 291 – 293.
[10] M. P. Andersson, F. Abild-Pedersen, *Surf. Sci.* **2007**, *601*, 649 – 655.
[11] J. Boah, P. Winchell, *Metall. Mater. Trans. A* **1975**, *6*, 717 – 724.
[12] W. Cribb, R. Reed-Hill, *Metall. Mater. Trans. A* **1978**, *9*, 887 – 890.
[13] S. Helveg, C. Lopez-Cartes, J. Sehested, P. L. Hansen, B. S. Clausen, J. R. Rostrup-Nielsen, F. Abild-Pedersen, J. K. Nørskov, *Nature* **2004**, *427*, 426 – 429.
[14] S. Hofmann, R. Blume, C. T. Wirth, M. Cantoro, R. Sharma, C. Ducati, M. Hävecker, S. Zafeiratos, P. Schnoerch, A. Oestereich, D. Teschner, M. Albrecht, A. Knop-Gericke, R. Schlögl, J. Robertson *J. Phys. Chem. C* **2009**, *113*, 1648 – 1656.
[15] D. Teschner, E. Vass, M. Hävecker, P. Schnoerch, S. Zafeiratos, H. Sauer, A. Knop-Gericke, R. Schlögl, M. Chamam, A. Wootsch, A. S. Canning, J. J. Gamman, S. D. Jackson, J. McGregor, L. F. Gladden, *J. Catal.* **2006**, *242*, 26 – 37.

